2012 IEEE/RSJ International Conference on
Intelligent Robots and Systems
October 7-12, 2012. Vilamoura, Algarve, Portugal

Design, Fabrication, and Modeling of the Split Actuator Microrobotic Bee

Kevin Y. Ma, Samuel M. Felton, and Robert J. Wood

Abstract— **The split actuator microrobotic bee is the first flight-capable, insect-scale flapping-wing micro air vehicle that uses "split-cycle" constant-period frequency modulation to control body forces and torques. Building this vehicle is an intricate challenge, but by leveraging a maturing fabrication technology for microscale devices, we have developed a solution to tackle the design and fabrication difficulties. We show that the design is able to independently modulate the motions of both wings and produce roll, pitch, and yaw torques, as well as a peak lift force of 1.3 mN, in a 70mg package.**

I. INTRODUCTION

Researchers and engineers have been developing insect-scale flapping-wing micro air vehicles (FWMAVs) for over two decades. As a culmination of nearly a decade of experience and developments, including innovations in custom actuators and micromanufacturing technologies, researchers were able to construct the Harvard microrobotic fly (HMF) [1], a 60mg, insect-scale vehicle that uses two flapping wings as its means to generate lift force. However, due to the limitations of the manufacturing technology at that time, the device only featured a single actuator driving the flapping motion of two wings and was unable to generate body torques for steering. Altitude control experiments were performed on the vehicle by constraining its motion to a single, vertical degree of freedom via guide wires [2]. These previous studies prove the feasibility of insect-scale FWMAVs; however, the lack of controlled body moments exacerbates the need for new designs.

The mechanical design space is large for FWMAV designs that can generate both forces and torques. Many configurations have the potential to work, and it becomes a question of which design is more capable or appropriate for certain applications. Constraints are varied: with the use of piezoelectric ceramic bimorph bending actuators [3] as in the HMF, the actuator mass is significant and managing that value is critical [4]. Jointly, the mass of the power electronics required to drive these actuators scale nonlinearly with actuator mass; due to concerns of electrical complexity, designs with fewer actuators may be favorable [5]. Certain body degrees of freedom may be deemed less critical than others, and an underactuated vehicle design may provide sufficient control authority with less actuator mass.

Biology can provide inspiration for the design of a controllable vehicle. Biologists have noted that fruit flies tilt the stroke planes of their flapping wings to make rapid turns while in forward flight [6]. Other researchers have identified wing hinge rotation modulation as the basis for fruit flies' ability to generate body torques [7]. Mechanical instantiations of these actuation configurations are entirely possible and waiting to be explored at the insect scale. The main concept in effect for these actuation schemes is modulation of each wing's angle of attack on a stroke-by-stroke basis.

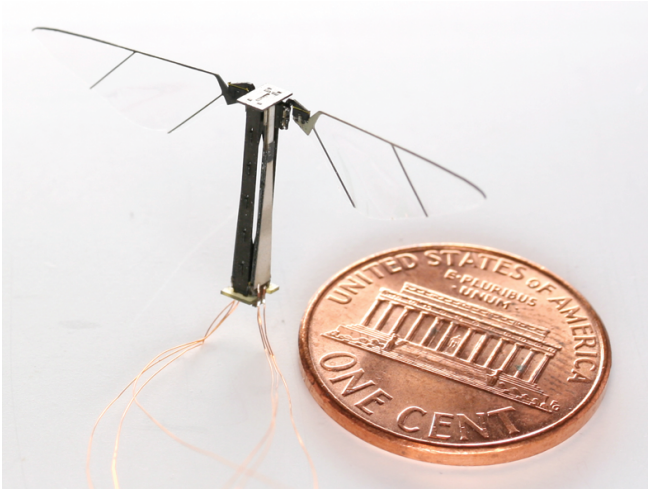

Fig. 1. The split actuator microrobotic bee.

Alternatively, a conventional vehicle engineering perspective can be applied, by abstracting the wing drive as a thrust force source. With two wings per FWMAV and thus two force sources, differential thrust forces can be generated bilaterally on the vehicle to induce body forces and torques. Differential force modulation can be accomplished in a number of ways. In one instance, Finio et al. took the established HMF design with a single power actuator and augmented it with control actuators – two smaller actuators integrated into each wing drive that can asymmetrically modulate stroke amplitude [8]. This design configuration, with three actuators total – two control and one power, was inspired by the thoracic mechanics in insects of the order Diptera, which separate power and control muscles [9]. It has proven to be capable of generating body torques on the vehicle [10].

Demonstrating another method of differential force modulation, the vehicle design presented in this paper uses two power actuators with each actuator independently driving a single wing, shown in figures 1 and 2. The actuation scheme and control strategy exhibited in this "split actuator bee" design, in reference to the legacy devices that have a

The authors are with the School of Engineering and Applied Sciences and the Wyss Insitute for Biologically Inspaired Engineering, Harvard University, Cambridge, MA 02138 kevinma@seas.harvard.edu

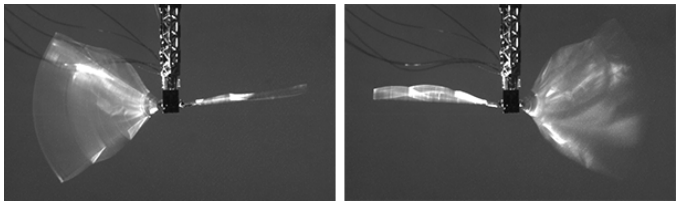

Fig. 2. The two wings of the vehicle can be controlled independently. In the left image, only the left wing is actuated. In the right image, only the right wing is actuated.

single power actuator driving both wings, has been explored extensively by Oppenheimer et al. [11], [12] (as well as demonstrated by Hines et al. for a larger scale flapper [13]). Oppenheimer demonstrated in simulation that two actuators could generate the required body torques and forces to provide sufficient control authority for six degree-of-freedom control – theoretically, the vehicle can be fully actuated. This two actuator control scheme was designated the "split-cycle" constant-period frequency modulation technique. The split actuator bee design presented in this paper is essentially the physical instantiation of that control scheme.

It remains to be seen which of these mechanical designs is superior for controlling insect-scale FWMAVs, or if different designs are better for different applications. One thing is certain: at this scale, manufacturing technology cannot be taken for granted. The split actuator bee design would not be possible to construct without the years of innovations in fabrication technology since the construction of the HMF [14], [15]. The precision, repeatability, and mechanical strength and fidelity of devices have drastically improved.

This paper describes the design and fabrication of the split actuator bee design and provides basic models to predict the dynamic behavior of the vehicle with this actuation scheme. Experiments are conducted to measure the body forces and torques that can be generated by the vehicle for a variety of control input signals. It will be shown that the split actuator bee is capable of generating all three body torques and thrust in excess of body mass.

II. DESIGN

The original Harvard microrobotic fly design [1] serves as the spring board for the split actuator bee design. It demonstrated that a vehicle with that combination of wings, actuators, mass, operating frequency, and transmission ratio, among other key features, could generate sufficient thrust force to lift off. The second iteration of the HMF [2], refined the design of the vehicle, leveraging advances in manufacturing technology to build a much more robust, repeatable design that was ultimately used in controlled altitude tests. Both the HMF and the split actuator bee use the same manufacturing technology for their mechanical components. The transmission mechanism is constructed from kinematic chains of rigid links and flexure joints as detailed in [14], [16]. The actuator is a piezoelectric bimorph actuator, constructed as described in [3]. A relevant fact for the following discussion is that the actuator is an oscillating,

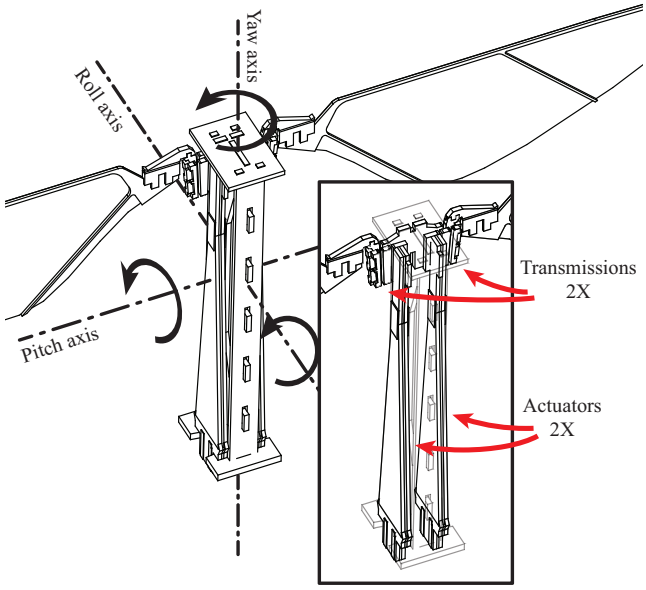

Fig. 3. Convention used to define the 3 body rotation axes. The insert highlights the use of two actuators and two wing drives in the vehicle.

bending cantilever beam with output taken at the distal end.

The split actuator bee design takes the HMF design and essentially splits the vehicle in half – the actuator is split into two separate actuators of equal base width and the two wings are decoupled and independently driven by each actuator. The geometry of each split actuator is such that the base width is half of the HMF actuator (1.75mm versus 3.5mm), but the actuator is optimized for energy density as detailed in [3] and retains an isosceles trapezoidal shape. Based on geometry of piezoelectric ceramic material alone, the total mass of the two split actuators is estimated to be 22% more than the single HMF actuator.

The single HMF actuator has sufficient power density to drive the load of two wings with appropriate wing trajectory and thrust generated. The key idea behind the split actuator design is that half of that single actuator should exhibit half of the force output to drive the load of a single wing, allowing a two-winged vehicle to achieve the same system performance. Approximating the flapping wing drives as linear second-order systems, halving the actuator would result in halving the system stiffness k. A single wing would have half the inertia and damping of two wings. Transmission dynamic effects are negligible. Resonant frequency is calculated as $\omega_n = \sqrt{k/m}$. Thus, the resonant frequency of a single split actuator wing drive should be similar to the two-wing drive. Assuming the mass of the auxiliary structures of the vehicle can be made similar or less, the split actuator bee should be able to attain a similar lift-to-weight ratio as the original HMF and have control authority over more body DOFs.

The primary mechanical design challenge for the split actuator bee is to robustly support two, kinematically decoupled wing drive mechanisms with an airframe that is stiff and low mass. A key design choice was how to orient the actuators

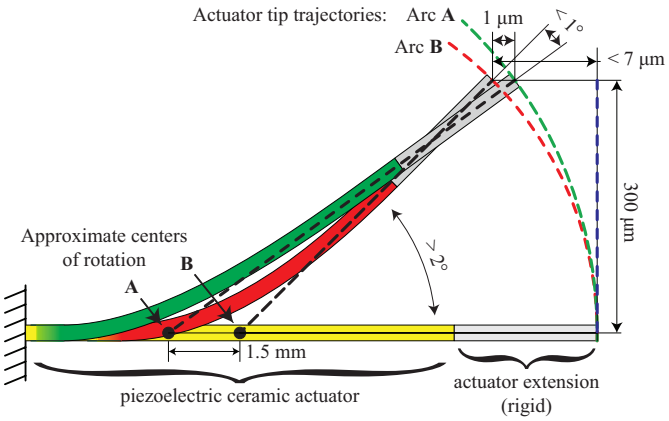

Fig. 4. Piezoelectric ceramic actuator bending profile indicating tip displacements and angles. The actuators can be approximated as a rotary motion source with a fixed center of rotation. A mismatch between the expected and actual (best approximation) center of rotation up to 1.5 mm has a negligible effect (maximum 1 μm tip offset, $< 1^\circ$ angular offset). (Beam deflections not to scale).

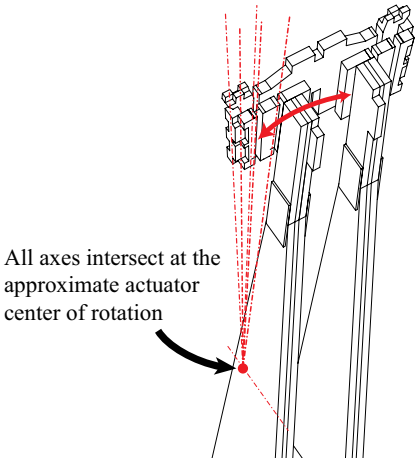

Fig. 5. Spherical four-bar illustration. All transmission joint rotation axes intersect at the approximate fixed center of rotation of the actuator. One four-bar for each actuator.

with respect to the motion of the wings. The straightforward choice would be to place the two actuators side by side with actuator tip motion in the dorsalventral direction, similar to the HMF. Instead, we took the opportunity to capitalize on the symmetry of the vehicle and cancel out the effect of each actuator's oscillating inertia by orienting the actuators to face each other, shown in figure 3. The actuators' tip trajectories are now in the lateral direction. If the actuators are oscillating in phase and with similar amplitude, the body torques due to their inertia should cancel out, assuming the actuators are well-grounded to the same rigid member. Oscillating actuator inertia has never been formally noted as a nuisance in these vehicles, but such body oscillations have the potential to decrease the effective wing stroke amplitude. This configuration of actuators will mitigate that possibility.

Another key insight in the mechanism design is that we can remove the slider crank from the transmission, saving space and weight in the vehicle. In the HMF, the slider crank converts the nominally rotary motion of the bimorph bending actuators to the linear motion that drives the planar four-bars of the transmission. That design was fixated on the actuator tip displacement, which is to first-order a purely prismatic motion, for small bending deflections. Rotary displacement is a second-order effect, as is the axial displacement of the tip. We normally drive the actuators to exhibit a 600μm peak-to-peak tip displacement. Large deflection beam bending theory predicts a 7μm axial displacement at the extremes of the tip trajectory. In the split actuator bee design, we do not fixate on the tip of the actuator, but instead look at the actuator bending profile as a whole. Here, it is more appropriate to approximate the actuator as a purely rotary displacement source with a fixed center of rotation. We empirically determined that the approximate center of rotation of the actuator output is 8mm from the tip, with a variation of 1.5mm between actuators. The precision of these measurements is not a major concern. Even if the mismatch between the expected and the actual center of rotation was 1.5mm at the extreme, the axial divergence of the actuator tip from the pure circular arc is on the order of 1 μm at maximum tip deflection, as illustrated in figure 4. This axial displacement can be tolerated and absorbed by the off-axis compliance of the flexure joints in the transmission.

Using the actuator as a rotary displacement source, we designed a transmission mechanism that consists of a spherical four-bar, with all joint rotation axes intersecting at a single point that is calculated to coincide with the approximate center of rotation of the actuator, illustrated in figure 5. The transmission ratio is designed to match the value in the original HMF. The actuator mates with the transmission along the edge of the last 3 mm of its length.

It is important to consider the requirements for energy efficiency when operating the vehicle; as shown in [1], operating at the resonant frequency of the system will enable maximum power efficiency. In the case of the split actuator bee, there are two, potentially different resonant frequencies – one for each wing drive. It is in our best interest to have the two resonant frequencies coincide, both for energy efficiency and symmetry of mechanical operation.

III. FABRICATION

The fabrication of these micromechanical systems has always been a big challenge and is one of the main obstacles facing the development of insect-scale FWMAVs. The split actuator bee design is a particularly difficult design challenge because the symmetry of the two halves of the vehicle is very critical for even basic operation. Granted, once the mechanism has been assembled, operation parameters will inevitably need to be separately tuned for both sides of the vehicle in order to achieve perfectly symmetric operation and repeatable flight behavior. However, those parameters can only be tuned to an extent established by the initial fabrication precision. It is therefore imperative to have both halves of the split actuator bee fabricated identically to maintain similar resonant frequencies. Only with recent

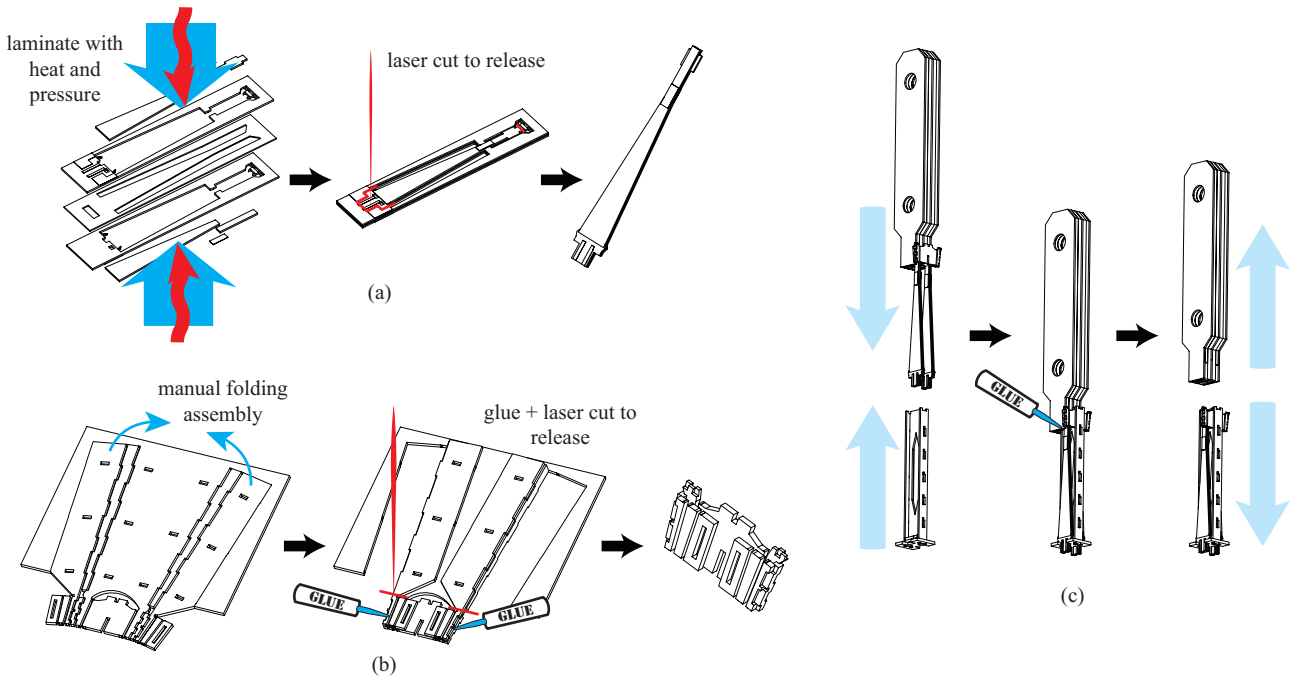

Fig. 6. Fabrication innovations used in the split actuator bee. (a) Piezoelectric actuator fabrication starts with mechanical alignment of components. Heat and pressure laminates the parts together. The epoxy resin in the carbon fiber middle layer serves as the adhesive. Laser cut to release actuator from the alignment structure. (b) Transmission fabrication involves an auxiliary structure to assist in precision folding. Manually fold, glue and laser cut to release. (c) Assembly of parts involves custom tools for precision alignment.

developments in the fabrication methodology and technology has this design been rendered practical to build. Recent advances in the Smart Composite Microstructures (SCM) process [16] have given us confidence in producing identical mechanical components. The actuator fabrication process has also been developed extensively since the HMF, and we can now confidently mass produce identical actuators. The only variable left to constrain is the variability in the assembly of the components.

We can be confident that the two, separate transmissions of the vehicle are the same. The fabrication of the transmission mechanism benefits from an assembly scaffold – a concept introduced in the MoBee [15]. The essential idea is that auxiliary, sacrificial mechanisms can be fabricated simultaneously around the intended mechanism for the sole purpose of removing degrees of freedom and assisting in precision assembly. In the case of the MoBee, the entire vehicle can be assembled by actuation of a single degree of freedom. This assembly approach is simple and elegant, but at the moment it is extremely time consuming to design. The split actuator bee takes a hybrid approach by using assembly scaffolds to assist in folding up the transmission mechanism only and relegating the other assembly steps to free hand manipulation. Other techniques employed in the precision fabrication of the mechanical components include extensive use of tabs and slots for mechanical alignment and custom alignment tools for assembly accuracy, seen in figure 6.

The production of the piezoelectric ceramic bimorph actuators is now much more repeatable. Prior art involved manually stacking miniscule, individual constituent material layers and placing into an opaque, vacuum-bagged setup with minimal assurance of retaining component alignment during part conveyance [3]. The new process uses the heated weight press and pin alignment, borrowed from the SCM process, to achieve very consistent results. The piezoelectric ceramic elements and alumina ceramic elements, used for the actuator extension, are cut out separately as pick-and-place components. These ceramics are 5mil thick plates of PZT-5H (Piezo Systems). A layer of 5mil FR4, fiberglass reinforced epoxy laminate, is machined with alignment features and clips to hold the smaller ceramic elements in place. This FR4 layer, along with the other layers of material, all include alignment pin holes which maintain the alignment of the layers during the heat press and cure step that bonds all the layers together. The actuator is then tested, prior to laser cut and release from the layup. These new fabrication techniques developed for the split actuator bee design are illustrated in figure 6a.

IV. MODELING

Researchers have noted that two-winged insects, such as the fruit fly, mainly rely on modulating their wings' angle of attack to perform flight maneuvers [6], [7]. While they utilize power muscles to maintain high-frequency wing flapping, they have a separate set of muscles used to control wing rotation about three axes [17]. In contrast, the split actuator bee design has only two actuators and can only modulate

wing flapping motion about a single axis. However, owing to the operation of the actuators, there is a great deal of control over that one degree of freedom, including flapping frequency, amplitude, bias of the mean stroke angle (wing bias), and asymmetry between up and down strokes in a single cycle ("split cycle"). In this manner, wing angle of attack is modulated indirectly, via passive rotation of the wing due to dynamic interactions with the air. Passive rotation of the wings was a design choice carried over from the HMF and has been shown as a viable solution for thrust force generation [18]. The basic model below demonstrates that using this actuation scheme, a flapping-wing device can generate thrust and achieve roll, pitch, and yaw body torques.

First, a linearized model is used to predict the damped resonant frequency of the system, which will define the operating frequency of the FWMAV. The derivation of the linearized system is fully detailed in Finio [8]. Gain G of the system is defined by the 2^{nd} order transfer function relating input voltage V to output wing displacement X, as a function of frequency ω.

$$G(\omega) = \left|\frac{X}{V}\right| = \left|\frac{A}{m_{eq}(j\omega)^2 + b_{eq}(j\omega) + k_{eq}}\right| \quad (1)$$

The equivalent mass, aerodynamic damping, and stiffness are lumped parameters, dependent on various physical parameters of the system which can be found in table I. Equivalent mass m_{eq} is dependent on the transmission ratio T, actuator mass m_a, and wing inertia J_ϕ. Damping b_{eq} is dependent on T, the radius of the center of pressure of the wing r_{cp}, and aerodynamic damping b. Stiffness k_{eq} is dependent on T, actuator stiffness k_a, and transmission stiffness k_t. The constant factor A is the proportion between input voltage V and output actuator force, dependent on physical parameters of the actuator. Based on this model and the values in table I, the damped natural frequency is calculated to be 104 Hz.

The input voltage signal controlling each piezoelectric actuator is a sinusoid characterized by amplitude V_{amp}, offset V_{off}, and a variable κ that defines the split cycle (figure 7). For the pair of actuators per vehicle, V_{avg} is the average of the two input signal amplitudes. Assuming the two signal amplitudes vary symmetrically about V_{avg} with variation V_{dif}, one actuator is driven with an amplitude $V_{amp} = V_{avg} + V_{dif}$ and the other actuator is driven with amplitude $V_{amp} = V_{avg} - V_{dif}$. The input signals are varied along $V_{avg}, V_{dif}, V_{off}$, and κ, to generate thrust and three torques on the vehicle. Equation 2 describes how these parameters influence wing displacement ϕ, in radians:

$$\phi = V_{off}G(0) + V_{amp}G(\omega) \cdot \begin{cases} cos(\frac{\omega t}{2\kappa}) & 0 < t < \kappa \cdot \frac{2\pi}{\omega} \\ cos(\frac{\omega t - 2\pi}{2(1-\kappa)}) & \kappa \cdot \frac{2\pi}{\omega} < t < \frac{2\pi}{\omega} \end{cases} \quad (2)$$

All forces exerted on the vehicle are assumed to come from the lift and drag forces on the wings. These forces are proportional to the square of the wing velocity $\dot{\phi}^2$, as well as drag and lift coefficients C_D and C_L, dependent on the angle of attack α [18]. To linearize the complex relationship between α and $\dot{\phi}$, α is treated as constant throughout the wing cycle, and equal to the optimal angle of attack for lift and drag, $\alpha_0 = 45°$. Because the frequency of wing flapping is much higher than the frequency of the body dynamics, the lift and drag forces can be treated as time averaged over the stroke period $P = 1/f = 2\pi/\omega$ (equation 3).

$$F_{L,mean} = \frac{1}{P}\int_0^P F_L = \frac{1}{4}\rho\beta C_L\left(\omega G(\omega) V_{amp}\right)^2 \quad (3)$$

ρ is air density and β is a constant representing the specifics of the wing planform geometry.

Thrust F_{thrust} is the sum of both wings' mean lift force magnitudes (equation 4). Roll torque τ_{roll} is the difference

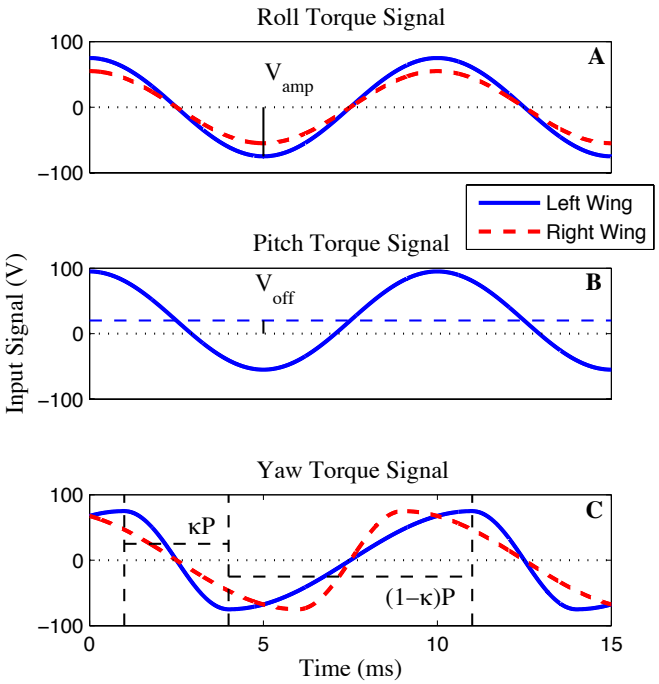

Fig. 7. Examples of signals that would be used to generate body torques on the FWMAV. The signals shown would activate: (A) roll torque by varying V_{dif} ($V_{dif} = 10$), (B) pitch torque by varying V_{off} ($V_{off} = 20$), and (C) yaw torque by varying κ ($\kappa = 0.3$).

TABLE I
PHYSICAL PARAMETERS

Parameter	Symbol	Value	Units
Actuator mass	m_a	25	mg
Wing inertia	J_ϕ	45.3	mg mm^2
Transmission ratio	T	3.333	rad/mm
Radius to center of pressure	r_{cp}	10.1	mm
Aerodynamic damping	b	2.03	μNs/m
Actuator stiffness	k_a	300	N/m
Transmission stiffness	k_t	5.09	μNm/rad
Equivalent mass[a]	m_{eq}	528	mg
Equivalent damping[a]	b_{eq}	0.228	Ns/m
Equivalent spring constant[a]	k_{eq}	356	N/m

[a]Relevant to the linearized model as described in [8]

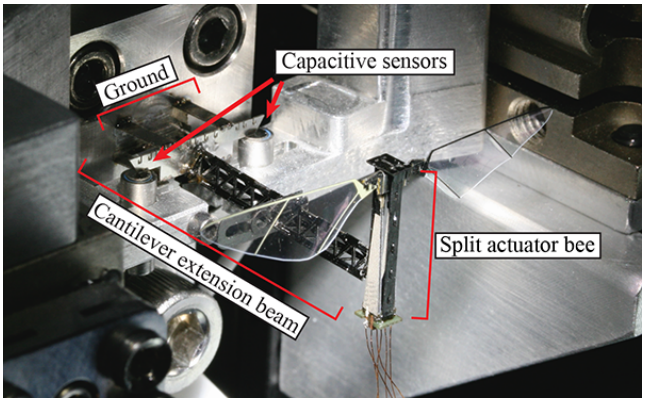

Fig. 8. The split actuator bee mounted on a custom dual-axis force-torque sensor. Measuring all three body torques requires remounting in different orientations. Here, the vehicle is mounted for roll torque measurements.

in mean lift force magnitude between the two wings. Recall the lift force is a function of $V_{amp} = V_{avg} \pm V_{dif}$.

$$\begin{aligned} F_{thrust} &= F_{L,left} + F_{L,right} \\ &= \frac{1}{2}\rho\beta C_L \left(\omega G(\omega)\right)^2 \left(V_{avg}^2 + V_{dif}^2\right) \end{aligned} \quad (4)$$

$$\begin{aligned} \tau_{roll} &= r_{cp}\left(F_{L,left} - F_{L,right}\right) \\ &= r_{cp}\rho\beta C_L \left(\omega G(\omega)\right)^2 \left(V_{avg} V_{dif}\right) \end{aligned} \quad (5)$$

Pitch torque τ_{pitch} is caused by the combined lift force vector of both wings offset from the vehicle center of mass in the foreaft direction. This offset is caused by a bias in the wing's mean stroke angle ϕ_{mean} (toward the front or back of the vehicle), which is proportional to V_{off} of the input signal.

$$\begin{aligned} \tau_{pitch} &= r_{cp} sin(\phi_{mean}) \left(F_{L,left} + F_{L,right}\right) \\ &\approx r_{cp} V_{off} G(0) F_{thrust} \end{aligned} \quad (6)$$

for small ϕ_{mean}.

Yaw torque τ_{yaw} is achieved through a difference in the drag force on the wing during up and downstroke. This is accomplished when the upstroke velocity is different than the downstroke velocity; larger drag forces occur during the quicker stroke. τ_{yaw} is dependent on κ, denoting the fraction of the cycle period that is occupied by the upstroke; $\kappa = 0.5$ indicates a pure sinusoid. The mean drag force of each wing is determined by integrating the drag force over the stroke period:

$$\begin{aligned} F_{D,left} &= -F_{D,right} \\ &= \frac{1}{P}\left[\int_0^{\kappa P} F_{D,upstroke} - \int_{\kappa P}^{P} F_{D,downstroke}\right] \end{aligned} \quad (7)$$

$$\begin{aligned} \tau_{yaw} &= r_{cp}\left(F_{D,left} - F_{D,right}\right) = 2 r_{cp} F_{D,left} \\ &= \frac{1}{8} r_{cp}\rho\beta C_D \left(\omega G(\omega) V_{amp}\right)^2 \left(\frac{1-2\kappa}{\kappa - \kappa^2}\right) \end{aligned} \quad (8)$$

V. RESULTS AND DISCUSSION

The completed split actuator bee weighs 70mg, comparable with the legacy 60mg HMF [1]. The vehicle was mounted on a custom dual-axis force-torque sensor consisting of a stiff cantilever beam and two capacitive sensors, shown in figure 8. This sensor can measure a single axis of torque and a single force perpendicular to the torque axis. To measure torque generation in three directions, the vehicle had to be remounted in different orientations. The resonant frequencies of the two wing drives on the vehicle were empirically determined to be approximately 95 Hz and 105 Hz. For each experiment, a 100 Hz signal (the average resonant frequency between the two wing drives) defined by $V_{avg}, V_{dif}, V_{off}$, and κ was input into the vehicle via a power tether for one second, and instantaneous force and torque were recorded at a sample rate of 10 kHz. The force and torque were averaged over the one second in order to give the measured force and torque.

In order to measure thrust and roll torque, the input signal's V_{avg} was discretely varied from 85V to 105V while the V_{dif} was discretely varied from -10V to 10V. When measuring pitch torque, V_{off} was varied from -20V to 20V, and when measuring yaw torque, κ was varied from 0.3 to 0.7.

Because fabrication variability can affect actuator properties, G was determined empirically by observing wing displacement at the operating frequency. This value was used in the models to predict thrust and torques.

To account for misalignments in mounting to the experimental setup and unavoidable fabrication asymmetries in the vehicle when collecting torque measurements, the measured torque was broken down into the activated torque τ_{act}, the distance of the vehicle's center of mass from the torque sensor's center r_{mis} times the thrust F_{thrust}, and a torque offset τ_0 due to differences in wing performance. r_{mis} and τ_0 were calculated via a linear fit of all data taken when the

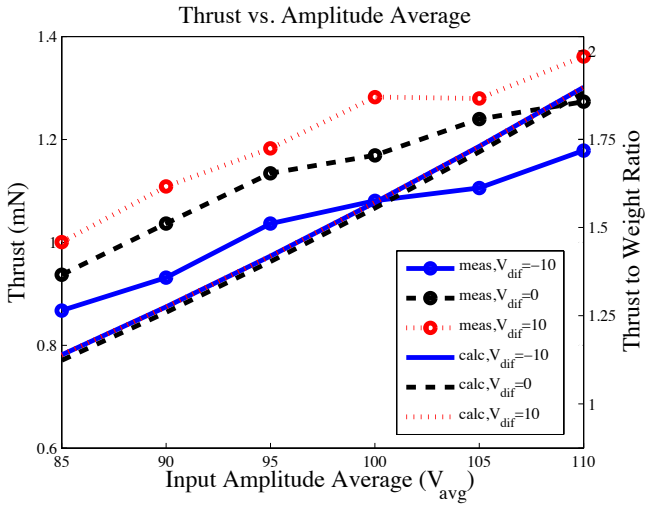

Fig. 9. Measured and calculated thrust as a function of the average signal amplitude V_{avg}. The thrust was observed with input amplitude differences between the wings V_{dif} of -10V, 0V, and 10V.

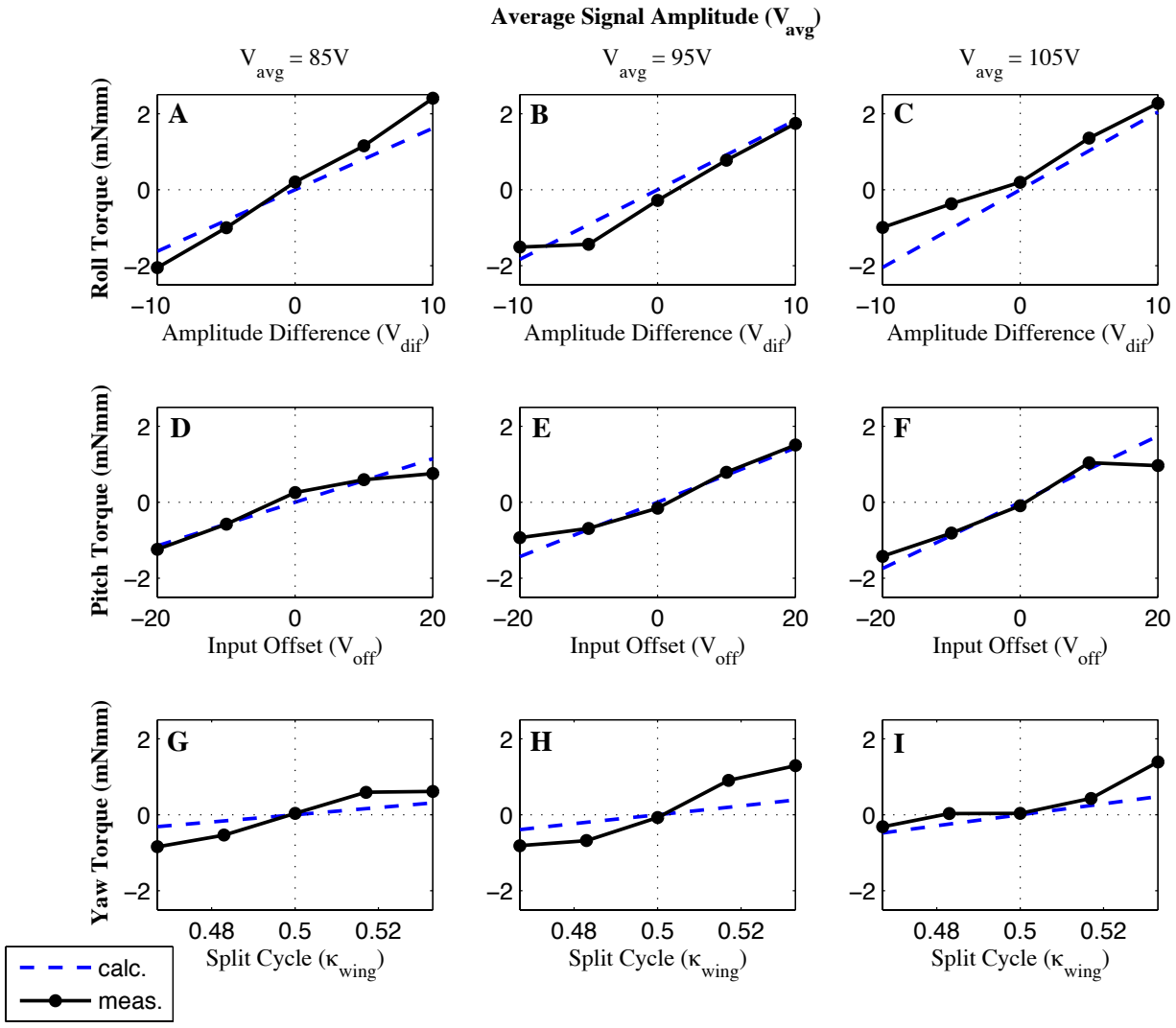

Fig. 10. Measured and calculated torques as a function of their corresponding signal variable. Each torque was observed when V_{avg} was 85V, 95V, and 105V. (A-C) Roll torque τ_{roll} is shown as a function of V_{dif}. (D-F) Pitch torque τ_{pitch} is shown as a function of V_{off}. (G-I) Yaw torque τ_{yaw} is shown as a function of κ_{wing}.

torques' dominant input variable (V_{dif},V_{off},κ) was inactive. The measured torque data was adjusted accordingly.

$$\tau_{measured} = \tau_{act} + r_{mis}F_{thrust} + \tau_0 \tag{9}$$

Figure 9 compares the measured thrust to the thrust expected by the model as a function of V_{avg}. Thrust shows a positive correlation with V_{avg}, with a maximum thrust of 1.36 mN, approximately twice the force necessary for the 70mg vehicle to hover. Contrary to the model, the increase in measured thrust as V_{dif} varies is much more pronounced. This was due to a fabrication error in the test vehicle that resulted in one of the wings performing better than the other in terms of force generation. Thus, a V_{dif} that favored the better performing wing cause the net thrust of the vehicle to increase.

Figure 10 shows the three measured torques at three different values of V_{avg}. In each case, the measured torque is plotted with the model's predicted torque. Each torque exhibits a positive correlation with the corresponding signal variable. We see that for roll torque τ_{roll}, the model is underestimating the torque generated. It also appears that the τ_{roll} range has a marked decrease for the high V_{avg} value. The pitch torque τ_{pitch} appears to match well with the model, except at the extreme values of V_{off}. All of these discrepancies between the model and the experimental data for roll and pitch torques seem to indicate that there is a breakdown in the linearity of the system as the wing drives reach the limits of their motion. This could be attributed to kinematic nonlinearity in the transmission four-bar or to nonlinearity in the input/output relationship of the actuators.

In the yaw torque τ_{yaw} case, the model is consistently underestimating the torque generated, indicating a lack of fidelity in the modeling. The experimental data also indicates a nonlinear relationship between the wing trajectory κ_{wing} and output τ_{yaw} – the increase in torque magnitude tapers

off for extreme κ's. Additionally, the asymmetry of the wing stroke, κ_{wing}, was observed to not match the asymmetry of the input signal, defined by κ. The input κ value of 0.3 resulted in the equivalent wing output κ_{wing} value of 0.467. Similarly, a $\kappa = 0.7$, which mirrors the assymmetry of $\kappa = 0.3$, resulted in $\kappa_{wing} = 0.533$. The system appears to be resisting deviations away from a sine wave, a characteristic of resonant mechanical systems. It is possible that κ is too simple a parameterization to define split cycle flapping, and a different parameterization is required to output the desired wing trajectories.

Concerning the magnitude of the body torques generated, the vehicle is on par with flight performance of fruit flies. Fruit flies have been observed to make 90° turns in less than 50 ms about their major inertial axis [6]. In the split actuator bee vehicle design, that corresponds to the roll axis. With a maximum measured roll torque of $3mN \cdot mm$ and an estimated maximum body inertia of $1.0322g \cdot mm^2$, the vehicle should be able to perform a 90° turn in 23 ms, by accelerating for 45° and decelerating for 45°. Granted, body drag due to angular velocity is not taken into account, but the performance is of the same order of magnitude as fruit flies. The measured torque generation capability of the split actuator bee also surpasses that of an alternative FWMAV design [10].

VI. CONCLUSION

The results prove that the split actuator bee vehicle design can generate body torques in the three rotational degrees of freedom. Each torque shows a positive correlation with the signal variable intended to modulate it. The linearized model of the system predicts the trends associated with input signals and output forces except for yaw torque, where the model underestimates the torque generated. The yaw torque model will need to account for more subtleties in the aeromechanical system. In addition, at the limits of wing motion, the linear model diverges from the physical system; the nonlinearities of the system will require further identification. Finally, we predict that the system dynamics are beyond what can be characterized by a single-input, single-output system. We have not investigated dynamic coupling between torques – a variety of experiments will need to be performed to gain an adequate perspective on its extent in the vehicle dynamics.

The results also show that the prototype vehicle used for the measurements was not symmetric. It is well within the capabilities of the manufacturing technology to construct a vehicle that has reliably symmetric operation. Future iterations will include precise "pop-up" mechanisms as featured in [15] to significantly curtail the amount of dexterous manual manipulation in the assembly process. Overall, the control authority afforded by this split actuator bee design should serve as a versatile test bed system for exploring how FWMAVs can perform flight maneuvers.

VII. ACKNOWLEDGMENTS

This work was partially supported by the National Science Foundation (award number CCF-0926148) and the Wyss Institute for Biologically Inspired Engineering. Any opinions, findings, and conclusions or recommendations expressed in this material are those of the authors and do not necessarily reflect the views of the National Science Foundation.

REFERENCES

[1] R. Wood, "Design, fabrication, and analysis of a 3dof, 3cm flapping-wing mav," in *Intelligent Robots and Systems, 2007. IROS 2007. IEEE/RSJ International Conference on*. IEEE, 2007, pp. 1576–1581.

[2] N. Pérez-Arancibia, K. Ma, K. Galloway, J. Greenberg, and R. Wood, "First controlled vertical flight of a biologically inspired microrobot," *Bioinspiration & Biomimetics*, vol. 6, p. 036009, 2011.

[3] R. Wood, E. Steltz, and R. Fearing, "Optimal energy density piezoelectric bending actuators," *Sensors and Actuators A: Physical*, vol. 119, no. 2, pp. 476–488, 2005.

[4] M. Karpelson, J. Whitney, G. Wei, and R. Wood, "Energetics of flapping-wing robotic insects: towards autonomous hovering flight," in *Intelligent Robots and Systems (IROS), 2010 IEEE/RSJ International Conference on*. IEEE, 2010, pp. 1630–1637.

[5] M. Karpelson, G. Wei, and R. Wood, "Milligram-scale high-voltage power electronics for piezoelectric microrobots," in *Robotics and Automation, 2009. ICRA'09. IEEE International Conference on*. IEEE, 2009, pp. 2217–2224.

[6] S. Fry, R. Sayaman, and M. Dickinson, "The aerodynamics of free-flight maneuvers in drosophila," *Science*, vol. 300, no. 5618, p. 495, 2003.

[7] A. Bergou, L. Ristroph, J. Guckenheimer, I. Cohen, and Z. Wang, "Fruit flies modulate passive wing pitching to generate in-flight turns," *Physical review letters*, vol. 104, no. 14, p. 148101, 2010.

[8] B. Finio, N. Pérez-Arancibia, and R. Wood, "System identification and linear time-invariant modeling of an insect-sized flapping-wing micro air vehicle," in *Intelligent Robots and Systems (IROS), 2011 IEEE/RSJ International Conference on*. IEEE, 2011, pp. 1107–1114.

[9] C. Williams and M. Williams, "The flight muscles of drosophila repleta," *Journal of Morphology*, vol. 72, no. 3, pp. 589–599, 1943.

[10] B. Finio and R. Wood, "Open-loop roll, pitch and yaw torques for a robotic bee," in *Intelligent Robots and Systems (IROS), 2012 IEEE/RSJ International Conference*. IEEE, 2012.

[11] M. Oppenheimer, D. Doman, and D. Sigthorsson, "Dynamics and control of a biomimetic vehicle using biased wingbeat forcing functions: Part 1-aerodynamic model," in *Proceedings of the 48th AIAA Aerospace Sciences Meeting Including the New Horizons Forum and Exposition, Orlando, Florida, USA*, 2010.

[12] ——, "Dynamics and control of a minimally actuated biomimetic vehicle: Part 2- control," 2009.

[13] L. Hines, V. Arabagi, and M. Sitti, "Free flight simulations and pitch and roll control experiments of a sub-gram flapping-flight micro aerial vehicle," in *Robotics and Automation (ICRA), 2011 IEEE International Conference on*. IEEE, 2011, pp. 1–7.

[14] J. Whitney, P. Sreetharan, K. Ma, and R. Wood, "Pop-up book mems," *Journal of Micromechanics and Microengineering*, vol. 21, no. 11, pp. 115 021–115 027, 2011.

[15] P. Sreetharan, J. Whitney, M. Strauss, and R. Wood, "Monolithic fabrication of millimeter-scale machines (accepted for publication)," *Journal of Micromechanics and Microengineering*, 2012.

[16] R. Wood, S. Avadhanula, R. Sahai, E. Steltz, and R. Fearing, "Microrobot design using fiber reinforced composites," *Journal of Mechanical Design*, vol. 130, p. 052304, 2008.

[17] M. Dickinson and M. Tu, "The function of dipteran flight muscle," *Comparative Biochemistry and Physiology Part A: Physiology*, vol. 116, no. 3, pp. 223–238, 1997.

[18] J. Whitney and R. Wood, "Aeromechanics of passive rotation in flapping flight," *Journal of Fluid Mechanics*, vol. 660, no. 1, pp. 197–220, 2010.